Exploring the Asymmetries of Pan-Tropical Connections from the Tropical Indian to the Pacific Basin

RAJASHREE NAHA,[a,b] SHAYNE MCGREGOR,[a,b] AND MARTIN SINGH[a,b]

[a] *School of Earth Atmosphere and Environment, Monash University, Melbourne, Victoria, Australia*
[b] *The ARC (Australian Research Council) Centre of Excellence for Climate Extremes, Monash University, Victoria, Australia*

(Manuscript received 14 November 2022, in final form 8 June 2023, accepted 27 July 2023)

ABSTRACT: Recent analysis of pan-tropical interactions suggests that post-1980 the tropical Indian Ocean's (TIO) influence on the tropical Pacific Ocean (TPO) appears to have subdued, while the tropical Atlantic Ocean's (TAO) influence has become more pronounced. The present study explores whether we can identify and dynamically explain any asymmetries in the pan-tropical connection between the TIO and TPO SSTs in an attempt to explain the recently reported weakening of the TIO influence. To this end, we carry out two idealized atmosphere-only experiments using the ACCESS atmospheric general circulation model where the sign of the decadal TIO SST signal is varied—presenting warm and cool TIO scenarios. We find a relatively strong asymmetric response of TPO precipitation to TIO SST anomalies, where average TPO precipitation shows a strong increase in response to TIO cooling, but a weaker decrease in response to TIO warming. The asymmetry is hypothesized to result from differences in the depth of latent heating over the TIO, which ultimately affects the depth of the remote response over the TPO. Asymmetries also occur in the spatial pattern of the changes in precipitation and surface winds. In the fully coupled system, these asymmetries would be expected to also alter the background state on which ENSO develops, providing a further mechanism by which the TIO influence may vary depending on its phase.

KEYWORDS: General circulation models; Climate variability; Decadal variability; Tropical variability

1. Introduction

El Niño–Southern Oscillation (ENSO) is commonly acknowledged as Earth's most dominant and important mode of interannual climate variability (McPhaden et al. 2006). Occurring in the tropical Pacific Ocean, ENSO is considered to be a coupled ocean–atmosphere phenomenon that is a result of a positive Bjerknes feedback (Bjerknes 1969) between anomalous western Pacific zonal winds and eastern equatorial Pacific sea surface temperature (SST). The phase of ENSO normally changes every 3–7 years, oscillating between El Niño, in which anomalously warm SSTs are observed across the central-eastern equatorial Pacific, and La Niña, in which anomalously cool SSTs are observed in that region. ENSO events are often accompanied by global tropical precipitation changes, which correspondingly have global socioeconomic impacts (McPhaden et al. 2006).

ENSO also displays pronounced decadal variability in the Pacific (Ault et al. 2013; Vimont 2005; McPhaden et al. 2020b; Power and Colman 2006). During the 1980s and 1990s, a number of large-magnitude ENSO events occurred (Trenberth and Hoar 1997; Timmermann et al. 1999, 2018); however, since the year 2000 we have seen more frequent, lower-amplitude events (Maher et al. 2014, 2018; Wang et al. 2019). The background state SSTs of the Pacific Ocean are thought to be important for understanding the apparent decadal changes in ENSO characteristics (Cai et al. 2001; Power et al. 2021; McPhaden et al. 2020a; Karamperidou et al. 2020). This decadal variability of the tropical Pacific [hereafter, tropical Pacific decadal variability (TPDV)] is largely considered to be driven internally (Liguori et al. 2020). Moreover, TPDV is also able to modulate the magnitude of global surface warming, with the recent acceleration of the trade winds being associated with the "hiatus" in global surface warming due to changes in internal storage of oceanic heat (Kosaka and Xie 2013; England et al. 2014). However, the precise drivers of these background state changes in the Pacific and their relationship to ENSO are still not fully understood (e.g., Power et al. 2021).

It is also believed that there is a two-way interaction between the variability of the tropical Pacific Ocean (TPO; 130°E–75°W, 20°N–20°S) with that of the tropical Atlantic Ocean (TAO; 75°W–30°E, 20°N–20°S) and the tropical Indian Ocean (TIO; 30°–130°E, 20°N–20°S). Focusing on the TPO/ENSO–TIO interactions for example, a developing El Niño can trigger a positive Indian Ocean dipole (IOD) by stimulating easterlies over the TIO and reduce the summer monsoon rainfall as a corresponding response to ENSO (Mishra et al. 2012).

It is also apparent that both the TAO and TIO feed back onto the TPO remotely, similar to how the TPO and ENSO forces variability in them (Kug and Kang 2006; Ham et al. 2013; Li et al. 2016; Wang et al. 2017). Focusing on the TIO–TPO connection for instance, TIO-induced Walker circulation changes are proposed to modulate the rapid termination of El Niño events (Kug and Kang 2006; Kug et al. 2006; Ohba and Ueda 2007; Luo et al. 2010; Okumura et al. 2011; Izumo et al. 2016) in much the same way as the atmospheric combination mode (C-mode) over the Pacific warm pool (which originates from the nonlinear atmospheric interaction

Corresponding author: Rajashree Naha, rajashree.naha@monash.edu

DOI: 10.1175/JCLI-D-22-0845.1

between ENSO and the Pacific warm pool annual cycle) is able to terminate El Niño events (McGregor et al. 2012, 2013; Stuecker et al. 2013; Abellán et al. 2018; Stuecker et al. 2015; Ren et al. 2016; Stuecker et al. 2017). However, statistical analysis suggests that these relationships have changed in the past. Moreover, in order to understand whether this is underpinned by something physical, we need to note that the TIO–TPO correlations may change due to random variations that can cause fluctuations and changes in the strength or pattern of these connections. These random variations can arise from the inherent chaotic nature of the atmosphere and ocean, as well as the influence of internal climate variability (Palmer 2019; Capotondi et al. 2018; Yun and Timmermann 2018; Kido et al. 2023).

In addition to the interannual perturbations, it has also been argued that the TIO SSTs alone can also affect the tropical Pacific basin rainfall and circulation patterns on decadal time scales and can cause atmospheric anomalies there (Xie et al. 2009; Tao et al. 2012; Luo et al. 2012; Cai et al. 2019; Wang 2019; Dhame et al. 2020). For instance, as a remote perturbation, the TIO SSTs are seen to affect the WP rainfall substantially (Ueda et al. 2015) and on decadal and multidecadal time scales the TIO warming can result in the generation of low-level easterlies in the WP and NWP, which further strengthens the Walker circulation and creates a La Niña–like response in the TPO (Kug and Kang 2006; Ohba and Ueda 2007; Zheng et al. 2011; Luo et al. 2012; Lee et al. 2020).

The TPO trade winds strengthened substantially around the turn of the millennium (Merrifield 2011; Luo et al. 2012; England et al. 2014). This recent trade wind intensification, which appeared to be inconsistent with other Pacific indicators (Li and Ren 2012), occurred alongside rapid TAO and TIO surface warming (Luo et al. 2012; McGregor et al. 2014; Li et al. 2016; Ruprich-Robert et al. 2017; Meehl et al. 2019), thus indicating a role for SST changes outside of the Pacific in this trade wind acceleration.

Decadal pantropical SST changes between the TAO and TPO and the TIO and TPO have been shown to play a role in modulating trade wind strength in the western Pacific (Cai et al. 2019; Wang 2019). The interbasin variability indices of a 20-yr sliding window suggest that after 1980 the trends of zonal wind stress in the western equatorial Pacific are more strongly correlated with the trends of SST differences between the TAO and TPO than with the trends of SST differences between the TIO and TPO (Cai et al. 2019). Moreover, it is also observed that since the 1990s significant warming in the west of the TIO has been directly linked to the significant weakening of the easterly wind anomalies in the western TPO (Han and Wang 2021). This recent strengthening of the TAO and weakening of the TIO modulation of western Pacific trade winds suggests that the strength of the influence of different basins on the TPO may have changed with time (Cai et al. 2019). Although some aspects of this interpretation have been confirmed by certain simulations with partially coupled models, there is still debate around which ocean basin is more dominant, and why these pan-tropical connections would change over time.

In this study we endeavor to investigate the decadal relationship between the tropical Indian and tropical Pacific basins in an attempt to shed light on the recent subdued connection between these two basins (Cai et al. 2019; Han and Wang 2021). The present study explores whether we can dynamically explain the recent weakening of the TIO–TPO connection on decadal time scales as identified by the reduced correlation between the TIO–TPO SST gradient with Pacific wind stress trends (Cai et al. 2019; their Fig. 3C). We utilize an AGCM to examine the impact of decadal TIO SST changes (exploring both warm and cool phases of the TIO) on the TPO atmospheric background state as ENSO is known to be sensitive to background state changes (e.g., Fedorov and Philander 2000). This experimental design allows us to understand the pan-tropical response without having to consider the TPO changes that would invariably come about in the coupled setting. Hence, this is able to provide a clear and intuitive understanding of what may be occurring to influence the recent TIO–TPO decadal relationship changes.

This article is organized as follows: section 2 details the model and experimental design, section 3 describes the tropical Pacific basinwide rainfall response and reports on the dynamics of rainfall changes, section 4 illustrates the regional response of precipitation, section 5 describes the regional wind response and its relationship to TPO precipitation changes, and last, section 6 presents the study's conclusions.

2. Model and experiment design

To determine the effects of TIO SST anomalies (SSTA) on the Pacific basin atmospheric circulation, including whether the Pacific response varies with the season, or the sign of the TIO SST changes, we carry out three sets of Atmospheric Model Intercomparison Project (AMIP)-style (prescribed SSTs) experiments. We use version 1.3b of the Australian Community Climate and Earth System Simulator (ACCESS) atmospheric general circulation model (AGCM) (atmosphere and land surface only) (Bi et al. 2013). The model is run on a 1.25° × 1.875° horizontal grid with 38 levels in the vertical. Each of our simulations covers the period between 1978 and 2001 based on the AMIP-II method of updating SSTs (Taylor et al. 2000) and includes 10 ensemble members. In all simulations, external forcings (e.g., aerosols, GHGs, etc.) are temporally evolving and daily and monthly average outputs are saved.

We carry out three sets of experiments that seek to explore the extent to which SST anomalies in the TIO are able to modulate the Pacific atmospheric background state. Each of these three experiments has the same SST forcing in the Pacific and Atlantic Oceans but has a different, temporally fixed pattern of SSTA (Figs. 1a,b) applied to the Indian Ocean region. Outside the tropics, we have imposed climatological SSTs and the SST signature that is applied to the TIO is concentrated only within the tropics (30°S–30°N) and tapers out linearly over 31°–34° north and south as we move poleward. In the TPO, the imposed SSTs are temporally evolving and taken from the AMIP simulated SST (Taylor et al. 2000) for the period 1978–2001. In the TAO, the SSTs do not evolve

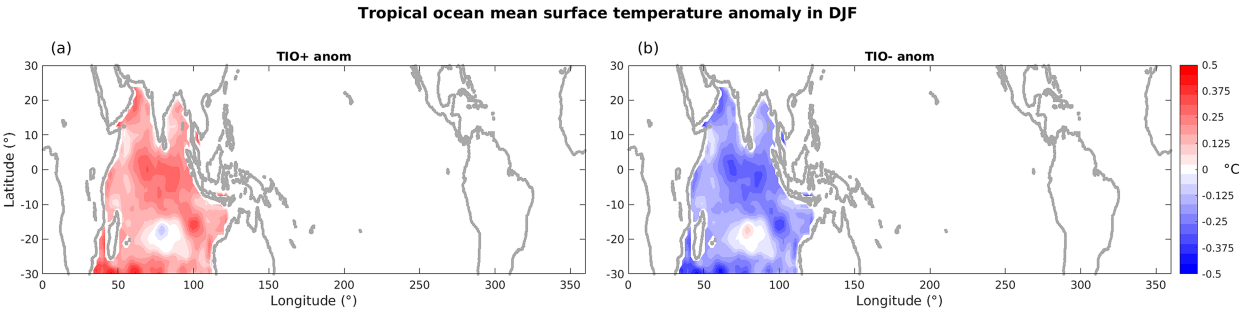

FIG. 1. Mean SSTA (°C) for the season DJF in (a) TIO+ minus control and (b) TIO− minus control.

with time and are given by the climatology calculated over the 1978–2001 period. The fixed pattern of TIO SSTA is calculated as the difference between the 1988–98 and 1999–2008 mean SST (Figs. 1a,b) using the NOAA Optimum Interpolation (OI) SST V2 dataset. This time period was selected as it had a large TIO basin wide average decadal SST difference (Fig. 5.2 in Naha 2022), and it also happened to straddle the period in which large Pacific Ocean trade wind acceleration occurred (England et al. 2014). This fixed TIO SSTA pattern is then multiplied by a constant, alpha ($\alpha = -1, 0, 1$), and added to the climatological TIO SST forcing (1978–2001), rendering our three experiments. The $\alpha = 0$ case is our "control" experiment, $\alpha = -1$ corresponds to TIO cooling (hereafter TIO−), and $\alpha = 1$ corresponds to TIO warming (hereafter TIO+), as illustrated in Fig. 1. Combined, these three AMIP-style experiments allow us to examine the impact of TIO SSTA on the TPO. A summary of the experimental design of the different TIO experiments is shown in Table 1 for reference.

3. The basinwide rainfall response

a. *Rainfall changes*

To explore the rainfall response of the TIO experiments, we first plot the long-term average seasonal cycle of TIO mean precipitation differences between the tropical Indian Ocean experiments (i.e., TIO+ and TIO−) and the respective control simulations (Fig. 2a). This analysis reveals that the TIO+ experiment acts to enhance TIO precipitation, while TIO− experiment acts to suppress TIO precipitation. These rainfall differences are found to be largest in the December–February months (as also supported by the fairly tight spacing of ensemble members during this period compared to JJA).

Of particular interest is the extent to which the response of the atmosphere to TIO variability is asymmetric between different phases of TIO—that is, whether the TIO+ experiment produces a rainfall response that differs in magnitude from the TIO− experiment. We assess the asymmetry in TIO phase here and elsewhere in this manuscript by determining if the response in the TIO+ experiment is significantly different to the response in the TIO− experiment. Here, the statistical significance of the response asymmetry between the TIO phases is calculated at the 95% confidence level using Student's t test, where we compared the response of TIO+ to that of TIO− with its sign flipped. In all the months (except April), the TIO+ precipitation response is larger than the TIO− response over the TIO basin. We find statistically significant TIO phase asymmetries (marked as colored shadings), where the TIO+ precipitation response is significantly larger than the TIO− response, in eight months (i.e., November–January, March, and June–September) (Fig. 2a).

Next, we consider the remote TPO rainfall response to TIO SST anomalies (Fig. 2b). In general, the TPO basinwide precipitation response suggests that TPO precipitation is enhanced in the TIO− experiment, while TPO precipitation is suppressed in the TIO+ experiment (both of which are consistent with our theoretical expectations) (Fig. 2b). However, the TIO+ experiment induced TPO rainfall decrease is very close to zero, as in all months some ensemble members are at or above the zero line. Assessing the significance of these changes we find that the TPO rainfall reduction due to TIO+ forcing is not significantly different from zero in any calendar month. On the other hand, the TIO− forcing is found to be significantly different from zero in all months. The TPO rainfall response to TIO− also appears to be larger in magnitude than the response to TIO+ in most months. This is supported by analyzing the statistical significance (at the 95% confidence level using Student's t test) of this response asymmetry between the two experiments (with the TIO+ response reversed when comparing with that of TIO−). It is apparent that there

TABLE 1. Summary of experimental design of the different TIO experiments. The climatological and total observed (climatology plus anomalies) SSTs are both from the period 1978–2001. The TIO SST anomaly (SSTA) is a fixed pattern calculated as the difference in mean SSTs between the two periods: 1988–98 and 1999–2008.

Ocean basin	Control	TIO+	TIO−
Tropical Atlantic Ocean (TAO)	Climatological SST	Climatological SST	Climatological SST
Tropical Pacific Ocean (TPO)	Observed SST	Observed SST	Observed SST
Tropical Indian Ocean (TIO)	Climatological SST	Climatological SST + TIO SSTA	Climatological SST − TIO SSTA

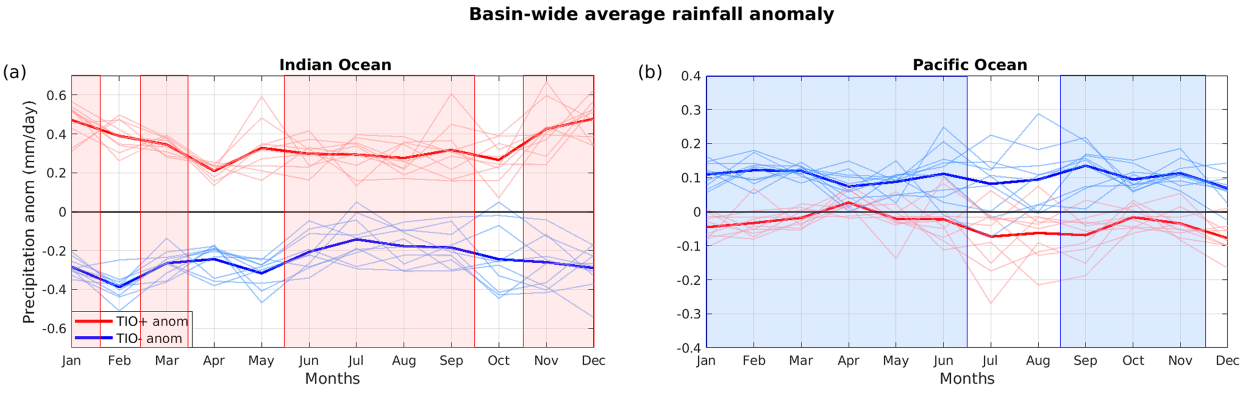

FIG. 2. Seasonal cycle of the basin average precipitation anomalies (1978–2001) over (a) the tropical Indian Ocean basin (40°–135°E, 20°N–20°S) and (b) the tropical Pacific Ocean basin (135°E–75°W, 20°N–20°S). The colored shadings in both panels indicate the statistically significant months at 95% confidence level (using Student's *t* test) for the TIO phase asymmetries. Here, the red shading indicates that the TIO+ response is larger than that of TIO−, while the blue shading represents that the TIO− response is larger than that of TIO+.

are significant asymmetries in most months, with the exception being July, August, and December (Fig. 2b).

b. *Dynamics of TIO rainfall changes*

Here we focus on the December–February period as this is the period with the most prominent TIO precipitation changes (Figs. 2a,b) but we note that similar results are found for other seasons (not shown). We see that the air temperature anomalies increase with height over the TIO for the TIO+ experiment while the anomalies decrease with height over the TIO for TIO− experiment (Fig. 3a). These temperature changes are due to the TIO warming in the TIO+ experiment, and they are associated with a local enhancement of convection, producing a positive diabatic heating anomaly in the troposphere. The simulated temperature anomalies are qualitatively similar to the temperature anomalies given by assuming moist adiabatic stratification (Singh and O'Gorman 2013), but they are somewhat asymmetric, with the magnitudes of the anomalies increasing with height more rapidly in the TIO+ case compared to TIO−.

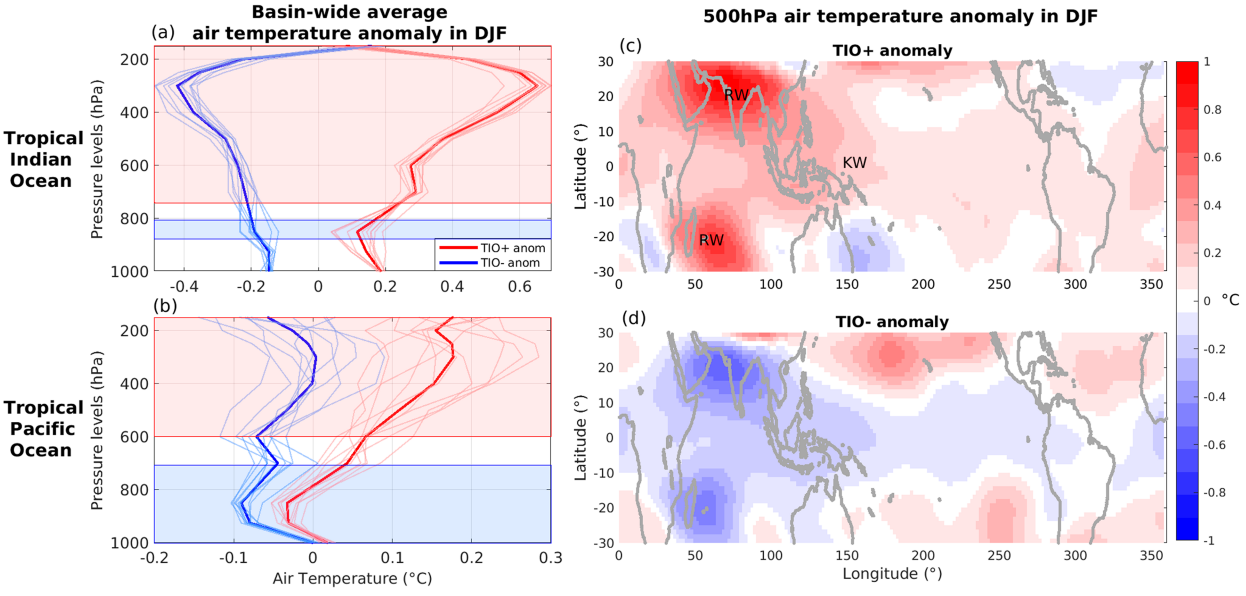

FIG. 3. Basinwide average (20°S–20°N) atmospheric temperature (°C) anomalies (TIO experiments minus control) vs pressure (hPa) over the (a) TIO and (b) TPO for the DJF season. The colored shadings in both panels indicate the statistically significant pressure levels at 95% confidence level for the TIO phase asymmetries (i.e., TIO+ compared to TIO− occurring at each pressure level) using Student's *t* test. Here, the red shading indicates that the TIO+ response is significantly larger than that of TIO−, while the blue shading represents that the TIO− response is significantly larger than that of TIO+. Midtropospheric (500 hPa) air temperature anomalies (°C) in the season DJF are shown for (c) TIO+ minus control and (d) TIO− minus control.

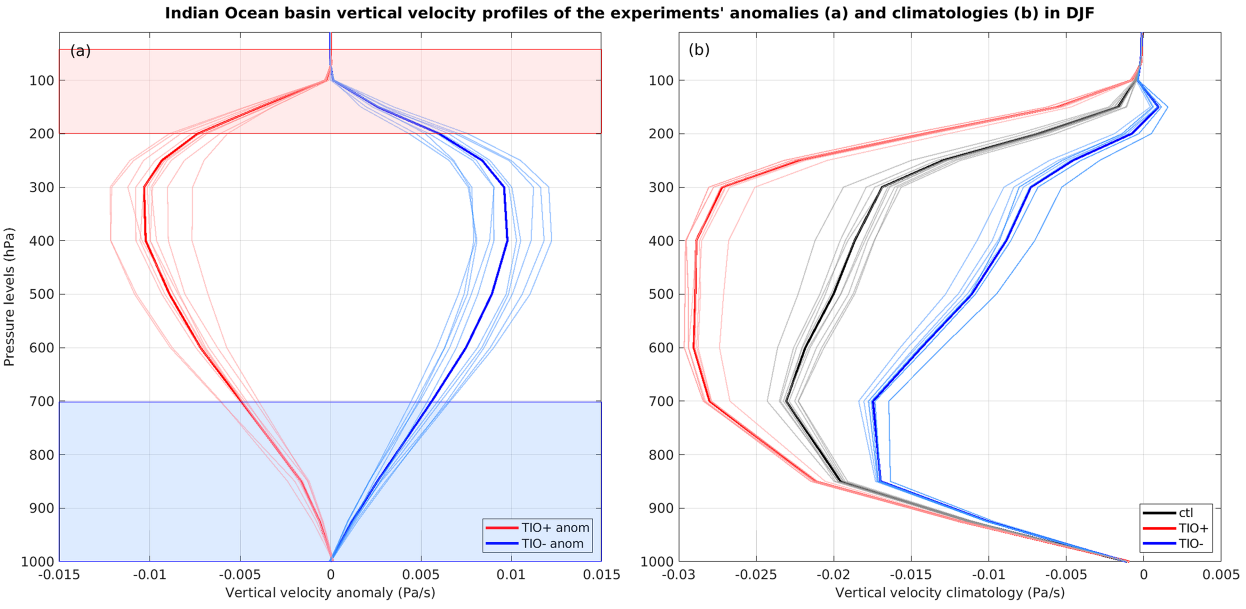

FIG. 4. Vertical velocity profiles in pressure coordinates (Pa s^{-1}) in the two experiments over the TIO region (40°–100°E, 25°S–5°N) in DJF showing (a) anomalies (TIO experiments minus control) and (b) climatological mean experiments. The colored shadings in both panels indicate the statistically significant pressure levels at 95% confidence level for the TIO phase asymmetries (i.e., TIO+ compared to TIO− occurring at each pressure level) using Student's *t* test. Here, the red shading indicates that the TIO+ response is larger than that of TIO−, while the blue shading represents that the TIO− response is larger than that of TIO+.

To further understand the modeled changes in convection in the two TIO experiments, we plot the vertical velocity (omega) profiles over the TIO region (40°–100°E, 25°S–5°N) in Fig. 4. The shape of vertical velocity profiles in the tropics is closely related to the profile of latent heating within clouds and therefore it is largely assumed to control the relative fraction of deep versus shallow convection (Back and Bretherton 2009; Inoue et al. 2020). While the two anomalous TIO vertical velocity profiles (TIO+ and TIO−) appear to be quite symmetrical, with both displaying magnitudes that increase with height up to around 350 hPa, this results in important changes in the total vertical velocity profile between these two experiments. The TIO+ experiment profile (red curve in Fig. 4b) displays a deep layer of strong vertical velocities, suggesting an enhanced possibility of a top-heavy latent heating profile (Back and Bretherton 2009; Inoue et al. 2020). Such top-heavy latent heating profiles have previously been associated with stratiform clouds characteristic of deep organized convective systems (Schumacher and Houze 2003b,a). Conversely, the TIO− experiment (blue curve in Fig. 4b) displays a decrease in vertical velocities above the 700-hPa layer, indicative of a shallower latent heating profile. As such, we would expect the TIO− experiment to largely produce low clouds and shallow convection in the TIO region (Back and Bretherton 2009; Inoue et al. 2020).

c. *Dynamics of TPO rainfall changes*

The rainfall response in the TPO opposes that of the TIO, and this may be qualitatively understood by considering a simple linear model of the equatorial response to diabatic heating anomalies placed in the TIO (Gill 1980). This TIO heat source results in the production of a Gill type response, which includes atmospheric Kelvin and Rossby waves propagating to the east and west of the heat source, respectively (Gill 1980). These waves alter the temperature structure of the entire tropical belt, thereby altering the stability in regions remote from the SST anomalies. As precipitation is strongly sensitive to atmospheric stability, the resultant changes in atmospheric stability provide a mechanism for the remote response of precipitation in different tropical ocean basins.

To examine the remote changes in stability, we consider the changes in Pacific basin average tropospheric temperature in the different TIO experiments (Fig. 3). While in the TIO+ experiment, the temperature response shows a stabilization throughout the TPO troposphere, in the TIO− experiment the TPO is only destabilized at low levels, with the temperature anomalies over the TPO being small above 700 hPa. As we discuss further below, the different depth of the response of the TPO temperature may be related to the differences in the depth of convection over the TIO in the experiments highlighted above.

Figures 3c and 3d display the spatial structure of TIO experiment temperature anomalies (TIO experiments minus the control) at 500 hPa during DJF. We note here that these 500-hPa air temperature spatial structures suggest that the TIO+ experiment leads to a more stable tropical Pacific atmosphere with higher temperatures aloft, while the TIO− experiment (Fig. 3d) leads to a less stable Pacific atmosphere with cooler temperatures aloft. This is also supported by Fig. 3b as well. In Figs. 3c and 3d, regional temperature signals are apparent emanating from the TIO basin that have characteristics consistent

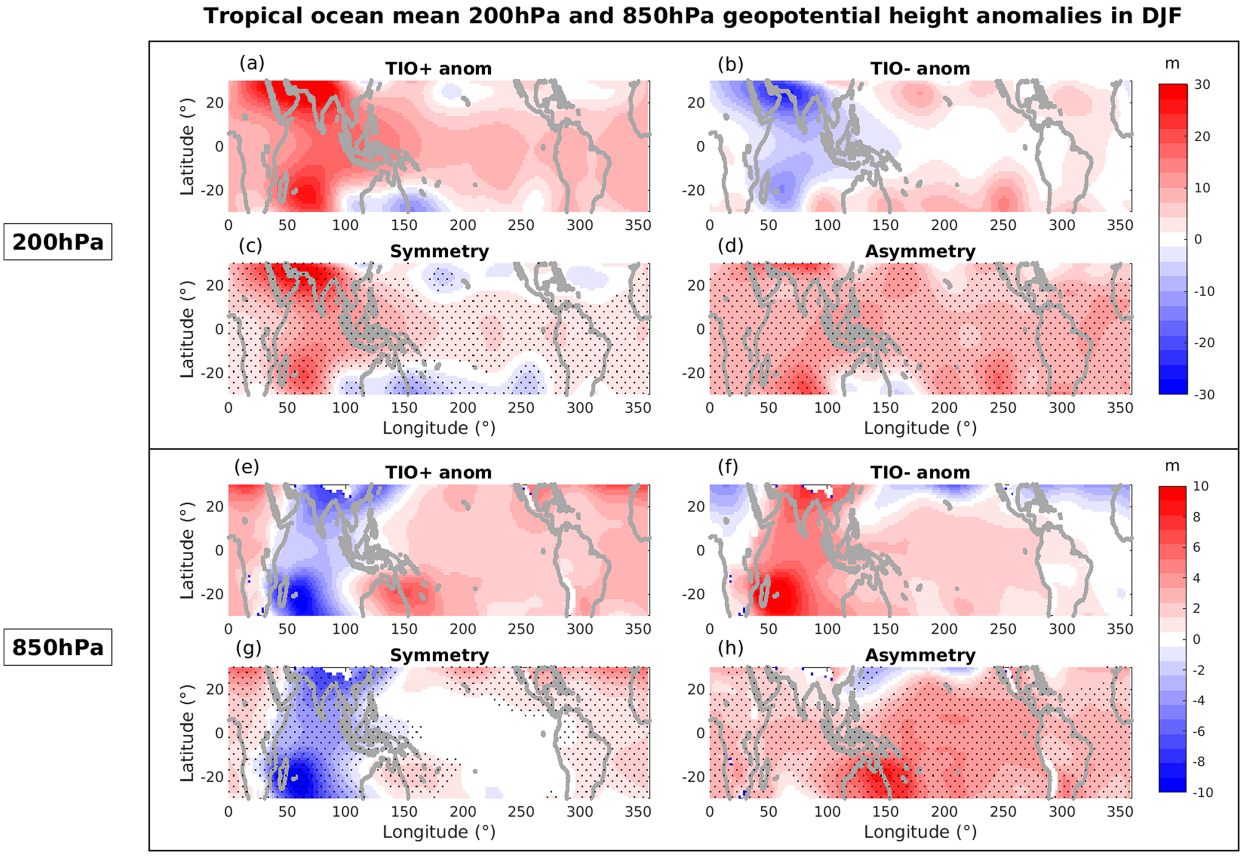

FIG. 5. DJF seasonal mean 200- and 850-hPa geopotential height anomaly (m) for the (a),(e) TIO+ anomaly and (b),(f) TIO− anomaly. Also shown are TIO experiment (c),(g) phase symmetries and (d),(h) phase asymmetries at 200 and 850 hPa, respectively. The regions that display statistically significant geopotential height differences at 95% confidence level in the symmetry and asymmetry maps in (c) and (d) are marked with gray stipples.

with westward propagating near-equatorial Rossby waves and eastward propagating equatorial Kelvin waves. In TIO+, the eastward propagating signals are seen to have a larger tropical Pacific basin magnitude and a broader meridional extent as compared to that of TIO−, which is again consistent with the temperature changes shown in Fig. 3b.

We then endeavor to better understand the atmospheric wave train (i.e., Kelvin and Rossby waves) response to the differences in the TIO convection between the TIO+ and TIO− experiments with the geopotential height at the lower and upper levels of the atmosphere. In Fig. 5, we plot the geopotential height anomalies at the 200-hPa (Figs. 5a,b) and 850-hPa (Figs. 5e,f) levels, also identifying the symmetrical (Figs. 5c,g) and asymmetrical components of the responses (Figs. 5d,h) in both experiments. Hereafter, the symmetric response is defined as (TIO+ minus TIO−) × 0.5, while the asymmetric response is defined as TIO+ plus TIO−. As such, the TIO+ experiment results are equal to the symmetric response plus 0.5 times the asymmetric response, while the TIO− experiment can be reproduced by the symmetric response minus 0.5 times the asymmetric response.

At 200 hPa, the geopotential height anomalies (Figs. 5a,b), exhibit anomalies that are extending from the west and east of the TIO heating due to SST-induced convection. The anomalies at the equator are consistent with an eastward propagating Kelvin wave emanating from the TIO basin as a response to the warming or cooling of the TIO basin (Gill 1980). The easterly extension of 200-hPa height anomalies in TIO+ stretches through the entire tropical Pacific belt (Fig. 5a), while that of TIO− appears to truncate on the western side of the Pacific, suggesting that the resulting Kelvin wave does not affect the whole tropical Pacific region (Fig. 5b).

Looking at the 850-hPa geopotential height anomalies, the TIO− experiment displays an anomaly extending eastward from the TIO heat source, which is consistent with an equatorial Kelvin wave (Fig. 5f), while TIO+ does not display this where the temperature anomaly is restricted to the TIO basin only and does not propagate eastward (Fig. 5e). This is almost the mirror image of what is occurring in the 200-hPa height anomalies (Figs. 5a,b). This suggests that the TIO− response is enhanced at lower pressure levels and reduced at higher pressure levels, suggesting that most of the circulation changes and cloud formation will be restricted to lower altitudes.

On the other hand, the TIO+ response is enhanced at higher pressure levels and reduced at lower pressure levels, suggesting that most of the circulation changes and cloud

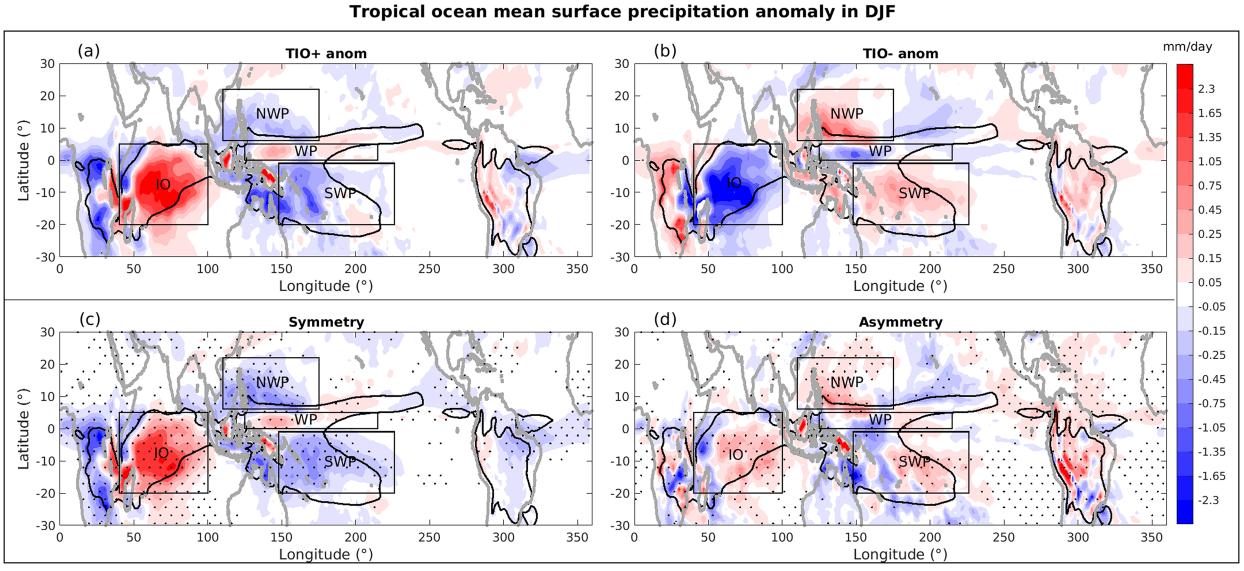

FIG. 6. DJF seasonal mean precipitation anomaly (mm day^{-1}) for the (a) TIO+ anomaly and (b) TIO− anomaly. Also shown are the TIO experiments phase (c) symmetries {i.e., [(a) − (b)]/2} and (d) asymmetries [i.e., (a) + (b)]. The regions that display statistically significant precipitation differences at 95% confidence level in the symmetry and asymmetry maps in (c) and (d) are marked with black stipples. The black boxed regions represent the different basin regions used in the text, namely, the Indian Ocean (IO; 40°–100°E, 20°S–5°N), northwestern Pacific (NWP; 110°–175°E, 6°–22°N), western Pacific (WP; 125°–215°E, 0°–5°N), and southwestern Pacific (SWP; 148°–226°E, 1°–20°S).

formation will be occurring at higher altitudes. One reason for this may be the shift in the vertical profile of ascent in the TIO shown previously (Fig. 4b). So we hypothesize that the symmetric response of ascent in the TIO gives asymmetric teleconnections because of how it alters the base state ascent profile (Fig. 4).

4. The regional rainfall response

We now endeavor to understand the spatial characteristics of the tropical precipitation response to the TIO perturbations including asymmetries with respect to TIO phase. Spatial patterns of the TIO-induced mean precipitation anomalies are shown in Figs. 6a and 6b, while their symmetrical and asymmetrical responses are presented in Figs. 6c and 6d.

The precipitation response in the TIO+ experiment largely mirrors that seen in the TIO− experiments (Figs. 6a,b), meaning that the precipitation response is broadly symmetric (Fig. 6c). For instance, in the TIO basin, there is a precipitation enhancement in TIO+ (Fig. 6a) and a precipitation suppression in TIO− (Fig. 6b). Also, over the African continent precipitation anomalies are negative in TIO+ (Fig. 6a) while they are positive in TIO− (Fig. 6b), a response consistent with previous studies (Funk et al. 2008; Dhame et al. 2020). Despite this apparent symmetry of the precipitation response over the TIO and Africa (Fig. 6c), statistically significant TIO phase asymmetries are also found in the TIO region (Fig. 6d), where the magnitude of the precipitation response is larger in the TIO+ experiment than the TIO− experiment.

It is observed that the warmest SST increases the subcloud moist static energy (MSE), which in turn is able to perturb the free troposphere resulting in high clouds and deep convection. Conversely, cool SSTs decrease MSE and may result in decoupling of the surface from the free troposphere thereby saturating the response [as seen in Figs. 3b and 3c in Williams et al. (2023)]. In this case, the atmospheric response to warm and cool SST perturbation will be asymmetric according to the "circus tent" model proposed by Williams et al. (2023). This mechanism helps to explain the asymmetric response of the TIO precipitation in our experiments (Fig. 6d).

Furthermore, it is seen that there is a slight mismatch between this TIO precipitation response, which is largely located south of the equator, and the symmetric Gill-type response (Gill 1980) apparent in Fig. 3. We believe that this discrepancy comes about as we focus on the DJF season, while the atmospheric response we are seeing could contain a lagged response to previous seasons (particularly in the Rossby waves). This view is supported by the TIO precipitation anomalies in SON being more symmetric about the equator than those seen in DJF (figure not shown).

The Pacific basin precipitation response largely agrees with the basinwide average in DJF, in that the TIO+ experiment largely displays precipitation decreases, which largely occur in the western/central Pacific. The TIO− experiment TPO precipitation response largely mirrors the TIO+ response, displaying precipitation increases in the western/central Pacific (Figs. 6b,c). Exemptions to these basinwide TPO rainfall changes, however, occur in the ITCZ region, where precipitation increases are seen in response to TIO+ and decreases are seen in response to TIO− (Figs. 6a–c). Furthermore, the asymmetrical response (Fig. 6d) suggests that there are differences between the experiments, especially in the northwestern and southwestern Pacific

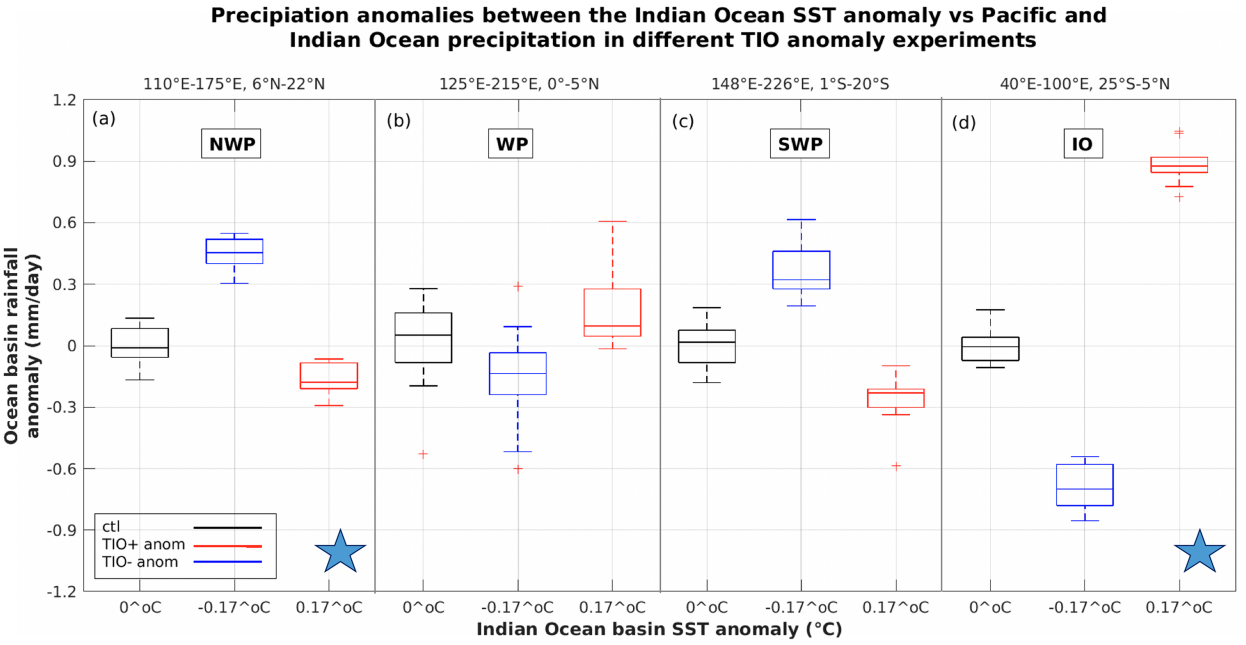

FIG. 7. Boxplots of the precipitation response in the different ocean basin boxed regions, namely, the (a) northwestern Pacific (NWP; 110°–175°E, 6°–22°N), (b) western Pacific (WP; 125°–215°E, 0°–5°N), (c) southwestern Pacific (SWP; 148°–226°E, 1°–20°S), and (d) Indian Ocean (IO; 40°–100°E, 20°S–5°N) in DJF. The black, blue, and red boxplots represent the control, TIO−, and TIO+ experiments respectively. The *x*-axis values are associated with the imposed SST anomalies in the different TIO experiments. The star symbols mark the regions when a significant TIO phase asymmetry exists in the precipitation response at 95% confidence level.

where strong statistically significant TIO phase asymmetries are found. The significant asymmetries in both of these regions suggest that the TIO− response is larger than the TIO+ response. This is the inverse of the symmetries seen in the TIO region. Evidence suggests that the precipitation changes in the TIO are driven by the changes in SST and associated MSE, while the precipitation changes in the TPO are largely driven by changes in stability.

To properly assess these apparent precipitation asymmetries to TIO phase, we have chosen several different ocean basin boxed regions, namely, the Indian Ocean (IO; 40°–100°E, 20°S–5°N) region in the TIO and the northwestern Pacific (NWP; 110°–175°E, 6°–22°N), western Pacific (WP; 125°–215°E, 0°–5°N), and southwestern Pacific (SWP; 148°–226°E, 1°–20°S) regions in the TPO (Fig. 6). These regions were selected because they either generally contained large precipitation anomalies or were somewhat distinct from the surrounding precipitation responses (Figs. 6a,b).

The average precipitation response in the IO boxed region (Fig. 7d) displays a statistically significant asymmetry, with the magnitude of the mean TIO+ response being approximately 29% larger than the TIO− response. This is just the opposite of the response seen in the NWP and SWP regions. In NWP region the precipitation response in the TIO− experiment is more than double (2.64 times) than that found in the TIO+ experiment (Fig. 7a). In the SWP region, on the other hand, the TIO− experiment is approximately 1.3 times the precipitation change found in the TIO+ experiment (Fig. 7a).

Reiterating, the TIO phase precipitation asymmetry is opposite for the TIO and the TPO basins. The TIO+ precipitation response in the IO boxed region is larger than that of TIO−, while the NWP and SWP regions display larger precipitation response for the TIO− than that of the TIO+ response. These changes are also supported by Fig. 6d as discussed previously. The TIO precipitation asymmetries are consistent with the air temperature profiles (Fig. 3a) of the two experiments, where over the TIO basin the TIO+ response is seen to be larger than that of TIO−. However, the TPO basin response appears more complex, with air temperature profiles (Fig. 3b) and geopotential height anomalies (Fig. 5) suggesting that the TIO− response is more focused at lower levels (below 500 hPa), while the TIO+ response is focused at upper levels. Further, the literature suggests that lower-level atmospheric stability changes are expected to be more strongly related to the precipitation changes (Yano and Plant 2012; Zhuang et al. 2017). This would further mean that due to the unstable atmosphere in TIO− below 800 hPa (Fig. 3b), there may be an enhanced precipitation response. However, it is not entirely clear if the temperature anomalies are leading to the precipitation response or vice versa as the temperature and precipitation anomalies generally depict a coupled response.

5. The regional wind response

In this section we seek to better understand the TPO surface wind response to TIO forcing, since, in the fully coupled system, it is the surface wind and surface wind stresses that

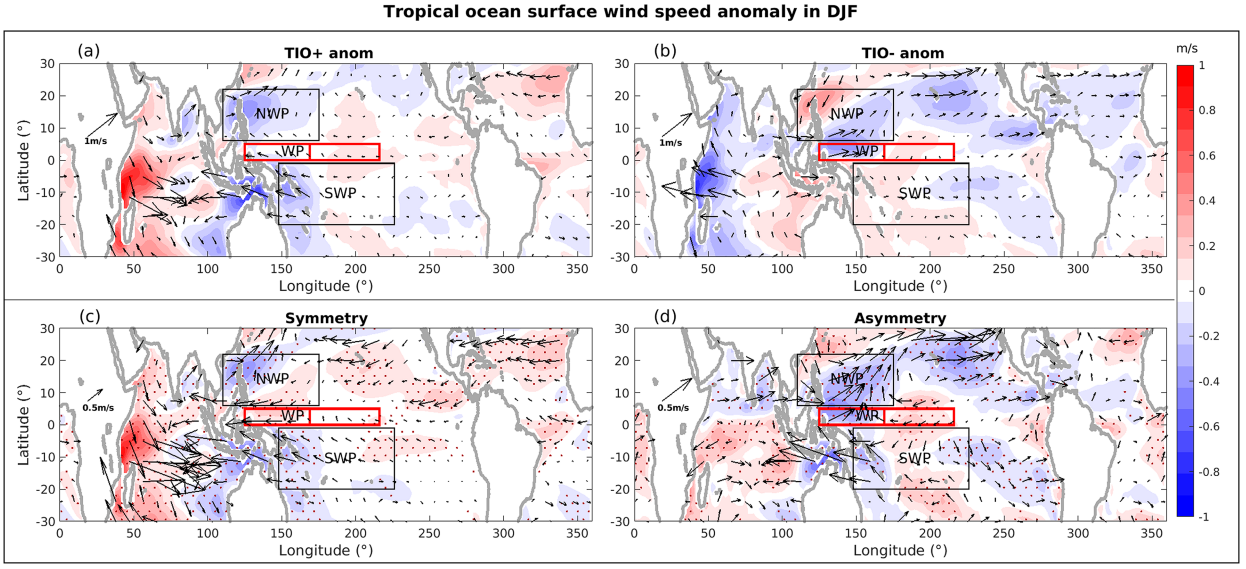

FIG. 8. DJF season mean anomalous winds (vectors) and wind speeds (contours) for (a) TIO+ and (b) TIO−. Also shown are the TIO experiment (c) phase symmetries {[(a) − (b)]/2}and (d) phase asymmetries [(a) + (b)]. The regions that display statistically significant wind speed differences at 95% confidence level in the symmetry and asymmetry maps in (c) and (d) are marked with maroon stipples. The black boxed regions represent the different Pacific basin regions used in the text, namely, the northwestern Pacific (NWP; 110°–175°E, 6°–22°N), western Pacific (WP; 125°–215°E, 0°–5°N), and southwestern Pacific (SWP; 148°–226°E,1°–20°S). The WP box is further divided into two sections as shown by the red boxed regions (125°–169°E, 0°–5°N and 169°–215°E, 0°–5°N).

drive oceanic heat flux and circulation changes, respectively. These two factors have led much of the recent literature on pan-tropical connections to focus on the atmospheric Walker circulation surface wind response to changing pantropical SSTA gradients (Ohba and Ueda 2007; Zheng et al. 2011; Luo et al. 2012; Dhame et al. 2020; Lee et al. 2020).

To this end, we analyze spatial patterns of the TIO-induced mean surface wind and wind speed anomalies in Figs. 8a and 8b along with their symmetric and asymmetric components in Figs. 8c and 8d. We note that the TIO basin wind speed response (Figs. 8a,b) shows a broad symmetry between the TIO experiments (Fig. 8c), with surface wind convergence occurring for TIO+ and divergence for TIO−. The symmetric wind response of the TPO includes easterly anomalies in the western equatorial and southwestern Pacific, while in the northwestern Pacific an anticyclonic feature is apparent (Fig. 8c).

In literature, it is reported that an IOB warming accelerates the decay of El Niño through enhanced convection over the TIO, which triggers anomalous easterlies in the WP and an anticyclonic anomaly in the NWP (Zheng et al. 2011; Okumura et al. 2011; Luo et al. 2012). These wind changes have a similar structure with the symmetric results presented in Fig. 8c. However, as our experiments model decadal changes, exactly how they would influence the individual ENSO events is a matter for further investigation.

It is also clear that there is a lot of asymmetry in the TPO between the experiments in terms of the wind changes (Fig. 8d). This is supported by the fact that the magnitude of the asymmetric response in the TPO (Fig. 8d) is of a similar magnitude to the individual experiment responses (Figs. 8a,b) and is much larger than the symmetric response in the TPO (Fig. 8c). The area west of 180° of the TPO largely displays the same sign wind speed changes (Fig. 8d) as the TIO+ experiment (Fig. 8a) suggesting that the TIO+ is having a stronger influence here than the TIO−. The exception here is the northwest Pacific region, which also has some similarities to the TIO− experiment and may result from a latitudinal shift of an anticyclonic (cyclonic) circulation feature apparent in the TIO+ (TIO−) experiment. The eastern half of the Pacific displays similar sign as that of the TIO− (Fig. 8b), suggesting that this part is affected more by TIO− than TIO+ (Fig. 8d). We also note that the surface wind changes appear to be stronger over the TIO basin in TIO+ than TIO− (Fig. 8d). The wind asymmetries (Fig. 8d) appear more pronounced and larger than those seen in the precipitation response (Fig. 6d). We note that many of these zonal surface wind asymmetries also exist at the 850-hPa level (not shown), indicating that they are dynamically driven by changes in geopotential height.

We now focus on the winds in the WP boxed region (0°–5°N, 125°–215°E) as shown in the previous figure (Fig. 8) as zonal winds in the western equatorial are known to be the relevant region for ENSO. As Fig. 8d also reveals strong TIO experiment asymmetries of different signs in the western and eastern sides of this WP box, we split the WP box into two smaller boxed regions with coordinates of 0°–5°N, 125°–169°E and 0°–5°N, 169°–215°E (as illustrated by the red boxed regions in Fig. 8). The TIO− displays a strong wind speed and zonal wind response in the west of the WP box (Fig. 8b), while the TIO+ response appears weaker (Fig. 8a). Conversely, in the eastern half of the WP box (169°–215°E, 0°–5°N) both the

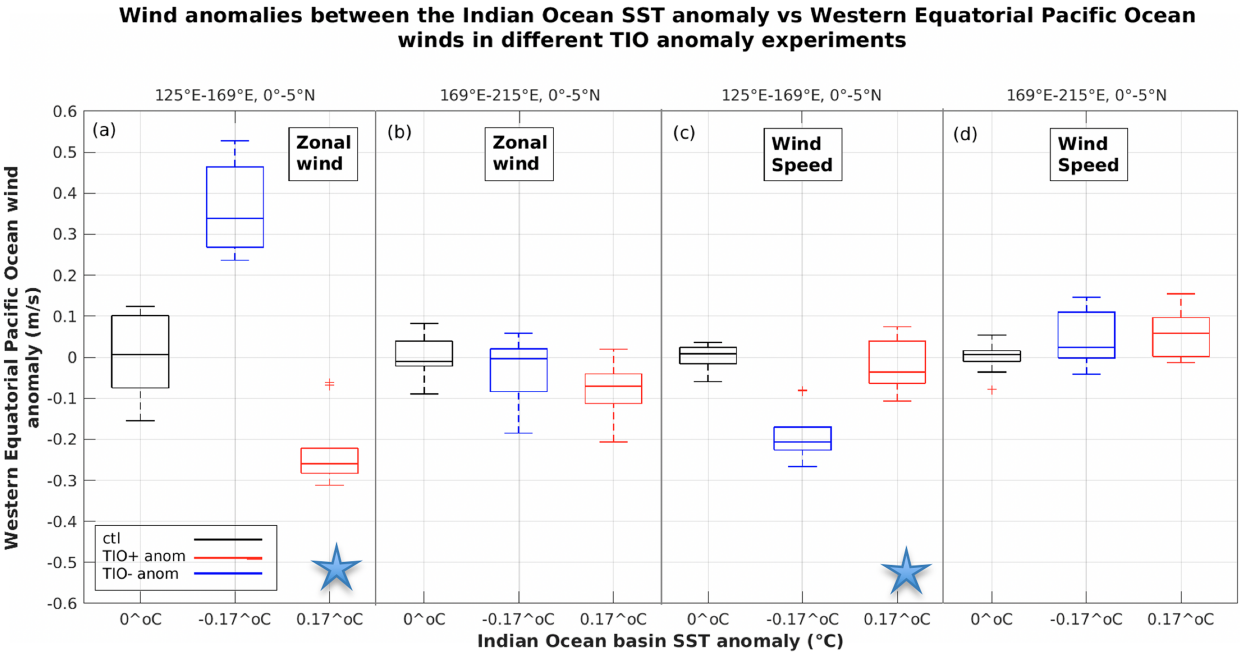

FIG. 9. Boxplots of the (a),(b) zonal wind anomalies (m s^{-1}) and (c),(d) wind speed anomalies in the two sections of the WP box (125°–169°E, 0°–5°N and 169°–215°E, 0°–5°N) as seen in the previous figure on surface wind speed responses (Fig. 8). The black, blue, and red boxplots represent the control, TIO−, and TIO+ experiments respectively. The *x*-axis values are associated with the imposed SST anomalies in the different TIO experiments. The star symbols mark the regions when a significant TIO phase asymmetry exists in the wind response at 95% confidence level.

TIO experiments display similar magnitude and sign of wind speed responses.

Moving forward with the analysis of the two subregions of the WP box, we plot the boxplots of zonal wind and wind speed anomalies in the two TIO experiments and in the two regions in Fig. 9. The west WP region reveals anomalous westerlies in TIO− (Fig. 9a) and weaker wind speeds (Fig. 9c), while in TIO+ there are anomalous easterlies (Fig. 9a) and little change to the wind speeds (Fig. 9c). The asymmetry in this region is highlighted by 1) the magnitude of the average TIO− zonal wind response being approximately 60% larger than the TIO+ zonal wind response and 2) the distribution of the zonal winds and wind speeds in the two TIO experiments displaying very little to no overlap. We also note that the fact that TIO+ does little to change wind speeds, despite the larger zonal wind changes, suggests that there is a partial compensation with meridional wind changes.

In the east of the WP box (169°–215°E, 0°–5°N), there is very little difference in the zonal winds (Fig. 9b) or wind speeds (Fig. 9d) between the two TIO experiments. That is, both of these experiments produce wind speed changes of the same sign and similar magnitude in this region, indicating another asymmetry. We note here, however, that the zonal wind and wind speed changes in the east WP region are much smaller than the wind changes seen in the west WP region.

Thus, during DJF in decades when the TIO is warm, we may expect anomalous easterlies to dominate the equatorial Pacific response. In these decades in DJF, this should lead to an equatorial Pacific region cooling due to the enhanced trade winds (stronger winds → more latent heat loss → local SST cooling) and easterly zonal winds (easterly wind anomalies → shoaling oceanic Kelvin wave → SST cooling in the eastern/central Pacific). Conversely, during DJF in decades when the TIO is cool we may expect warming of the equatorial Pacific region due to the weakened trade winds (weaker winds → less latent heat loss → local SST warming) and westerly zonal winds (westerly wind anomalies → deepening oceanic Kelvin wave → SST warming in the eastern/central Pacific).

Literature suggests that ENSO is sensitive to the background state thermocline depth, with its zonal mean (McPhaden et al. 2006; Neelin et al. 1998; Fedorov and Philander 2000; Zhang et al. 1997) and tilt potentially playing a modulating role (Yeh et al. 2009; Capotondi and Sardeshmukh 2015). As such, the TPO response to TIO SST forcing is further investigated with a linear ocean "shallow water" model (SWM) (McGregor et al. 2007; Neske and McGregor 2018). These SWM experiments are forced with a repeating anomalous annual cycle of wind stress differences (experiment minus control) from the two TIO experiments (alpha = −1, 1) for 20 years. The SWM is a linear (two-dimensional) first baroclinic-mode (shallow-water) ocean model in which the wind stress–driven active upper layer is separated from the infinitely deep motionless lower layer by a sharp tropical pycnocline, which is taken to approximate the tropical Pacific thermocline [details on the SWM equations can be found in Neske and McGregor (2018), their Text S1]. As such, the modeled changes in zonal average equatorial thermocline could underpin changes in ENSO (Fedorov and Philander 2000), the central Pacific thermocline depth changes could

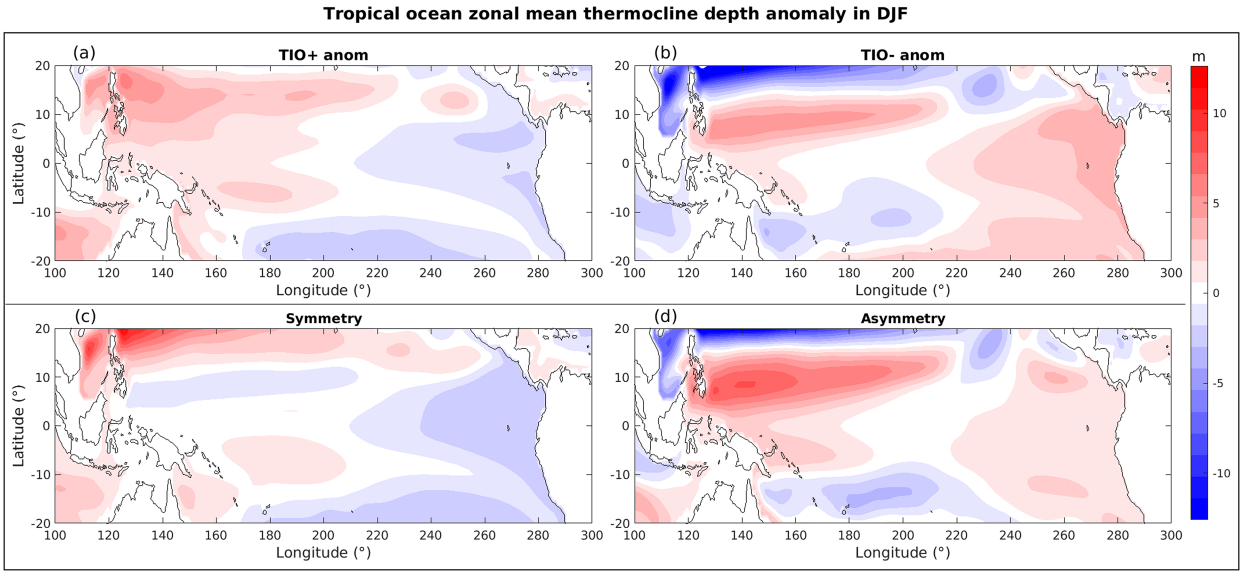

FIG. 10. DJF season shallow water model (SWM) mean thermocline depth anomaly (m) for the (a) TIO+ anomaly and (b) TIO− anomaly. Also shown are the TIO experiment (c) phase symmetries and (d) phase asymmetries.

influence the ENSO event flavor (Capotondi and Sardeshmukh 2015), and the eastern Pacific thermocline depth changes, where there is a clear direct connection with the overlying SSTs (Zelle et al. 2004), may be directly related to changes in the overlying SSTs and differences in the zonal temperature gradient.

In our experiments, we see that the added TIO forcing modulates the equatorial region thermocline depth (Fig. 10). TIO+ produces a zonal mean tilt (Fig. 10a), which is shallow in the eastern Pacific and deep in the western Pacific, while the TIO− produces deepening in the eastern and western equatorial Pacific consistent with a zonal mean deepening as seen in Fig. 10b.

Looking to the symmetric TPO response of the equatorial thermocline depth changes, these are mostly concentrated in the EP region, where the experiments show a somewhat consistent response. TIO+ leads to a shoaling of the eastern Pacific thermocline depth, while TIO− leads to a deepening of the eastern Pacific thermocline depth. These changes are consistent with the previous assumptions about the TIO+ winds (Figs. 8 and 9) leading to La Niña–like cooling in the eastern/central tropical Pacific (Figs. 10a,c). On the other hand, TIO− winds were expected to lead to an El Niño–like warming of the central/eastern tropical Pacific due to the relatively deep EP thermocline depth (Fig. 10b). Quantitatively, these decadal changes in the eastern tropical Pacific thermocline depth are relatively large, being approximately 1/3 of the size of SWM thermocline depths in the region related to the first EOF mode of a simulation forced with observed anomalous wind stresses over the period 1958–2002 (Fig. 13 of McGregor et al. 2012).

Plotting the asymmetrical response between the two TIO experiments, we see that the WP region shows relatively strong responses (Fig. 10d). These asymmetries extend to the northwest equatorial Pacific (Fig. 10d), where very strong asymmetries exist. In these regions, both experiments produce a deepening thermocline response in the region, making it highly asymmetric. The thermocline deepening signal in the northwest equatorial region is apparent in both TIO experiments in this region; it appears more poleward stretched or shifted in TIO+ (Fig. 10a) than TIO−. This could be related to the poleward shift of the NWP anticyclone in TIO+ (e.g., Wang et al. 1999).

Utilizing linkages between the mean state and variability of ENSO based on conceptual models, these TIO-induced changes in the zonal tilt and zonal mean thermocline depth (Table 2) would be expected to lead to changes in the period and growth rate of ENSO (Fedorov and Philander 2000). We see that both TIO+ and TIO− are responsible for the zonal tilt (Table 2) and are expected to lead to changes in ENSO growth rate (Fedorov and Philander 2000), although the TIO+ response in terms of zonal tilt is relatively larger than TIO−. Moreover, TIO− largely contributes to the zonal mean changes (Table 2), leading to changes in ENSO period (Fedorov and Philander 2000), while the TIO+ response in terms of zonal mean changes is almost negligible. These equatorial thermocline depth changes are also expected to modulate the mean state circulation in the Pacific, properties of water exchanged between the extratropics and tropics, and

TABLE 2. Tropical Pacific Ocean mean thermocline depth (m) as a difference between the west (120°E–155°W, 5°S–5°N) and the east Pacific (155°–80°W, 5°S–5°N) in the two TIO experiments in DJF. The bold values indicate the largest responses (shoaling or tilting) between the two TIO experiments.

Tropical Pacific Ocean	TIO+	TIO−
Zonal mean change (shoaling) (m)	−0.106	**2.581**
Tilting (m)	**2.334**	−1.803

SSTs. There are also certain off-equatorial changes where large TIO changes and phase asymmetries are displayed (Fig. 10d) and these warrant further investigation with a full ocean model.

6. Conclusions

Motivated by observed decadal variations in interbasin interactions affecting the Pacific, this study used AMIP-style experiments to explore the response of the tropical Pacific Ocean (TPO) to SST forcing in the tropical Indian Ocean (TIO). Specifically, we investigated the extent to which the TPO precipitation and surface wind responses were symmetric with respect to the sign of imposed TIO SST anomalies.

Consistent with observations and previous modeling studies, positive SST anomalies in the TIO enhance the precipitation in that basin, while negative SST anomalies act to suppress it. While the strength of the TIO precipitation response was broadly linear with respect to the magnitude of the SST anomalies, positive SST anomalies produced a slightly larger response than negative SST anomalies in the TIO basin.

The precipitation changes in the TIO are associated with diabatic heating anomalies in the atmosphere that can produce remote effects on the circulation (Gill 1980), ultimately resulting in precipitation changes in other basins. In our simulations, we find that, consistent with a Gill-type response, warming in the TIO suppresses precipitation in the TPO and stabilizes the atmosphere there. Spatial patterns of the precipitation response reveal that the TPO changes largely occur to the west of 160°W, though a small opposite signed signal is also apparent along the ITCZ region. A distinct asymmetry is identified in the TPO precipitation response, whereby the TPO precipitation response to TIO+ is much smaller in magnitude than that of the TIO−. Spatially, this is most clearly apparent in the northwest Pacific. It is interesting to note that the precipitation asymmetries in the TPO are opposite to those in the TIO. That is, the TIO basin precipitation response to TIO+ forcing is larger than its response to TIO− forcing, while the reverse is seen in the TPO where the TIO− response is larger than that of TIO+ response.

As to why the TPO displays an asymmetric precipitation response, we hypothesize that this is due to differences in the depth of convection over the TIO between the TIO− and TIO+ experiments (Fig. 3b). In the TIO+ experiment, large-scale ascent in the TIO displays a top-heavy structure, characteristic of deep convection, and a high fraction of stratiform clouds. In the TIO− experiment, the profile of ascent is substantially more bottom heavy. These differences are likely to lead to differences in the depth of the associated latent heating, producing remote effects at different depths in the troposphere. Indeed, the TIO− experiment has a large TPO temperature response below around 700 hPa, relative to the TIO+ experiment. On the other hand, above 700 hPa, the TIO+ experiment TPO air temperature increases prominently with height (indicating a more stable atmosphere), while the TIO− experiment air temperatures tend to zero (indicating no real change in stability). These results suggest that the remote atmospheric response to TIO− occurs nearer to the surface than the atmospheric response to TIO+. The differences in the depth of the remote TPO response ultimately produce asymmetries in the TPO precipitation response. The mechanisms for this asymmetry are complex, but we speculate that because precipitation responds particularly strongly to near-surface stability changes (Yano and Plant 2012; Zhuang et al. 2017), this may lead to a stronger precipitation response in the TIO− case.

The TIO perturbations also lead to strong wind changes over the western Pacific in our simulations that may have important implications for ENSO variability (Weisberg and Wang 1997). In particular, the TIO− produces anomalous westerlies (Fig. 9a) and weaker wind speeds (Fig. 9c) in this region, while the TIO+ produces anomalous easterlies (Fig. 9a) and stronger wind speeds (Fig. 9c). This result is broadly consistent with earlier works that seek to understand the role of the TIO in the termination asymmetry of individual ENSO events (Okumura et al. 2011). However, we also identify some clear asymmetries in the winds of this region which appear to be dynamically driven, whereby the TIO− displays a statistically stronger surface zonal wind response (Fig. 8b) than the TIO+ (Fig. 8a). The asymmetric response to TIO SSTA forcing identified in our experiments has not been raised in previous studies. If this asymmetry exists on interannual scales, it may actually act to counteract the TIO−TPO asymmetry proposed by Okumura et al. (2011) to cause the duration asymmetry between the El Niño and La Niña events. In that study it was suggested that the western equatorial Pacific wind response was linear to both a TIO warming and cooling, while the asymmetry was underpinned by differences in the zonal wind response between El Niño and La Niña events.

Initial investigations of the potential oceanic response of the TPO to TIO forcing are carried out with a linear oceanic shallow water model (SWM). These simulations reveal that the TIO-induced TPO wind changes consistently modulate the eastern equatorial Pacific thermocline depth, inducing shoaling of the thermocline for TIO+ and deepening for TIO−. As thermocline depth changes in the eastern Pacific are strongly related to changes in overlying SSTAs (Zelle et al. 2004), we would expect a SSTA signature of these thermocline depth perturbations. Thus, the wind perturbations induced in TIO+ would be expected to lead to a La Niña–like background state cooling, while TIO− winds would lead to El Niño–like background state warming. Similar responses to Pacific wind stress changes have been argued to be present in previous studies (Fedorov and Philander 2000; Capotondi and Sardeshmukh 2015). Furthermore, utilizing linkages between the mean state and variability of ENSO based on conceptual models, it is shown that the TIO-induced changes in the zonal tilt and zonal mean thermocline depth (Table 2) would be expected to lead to changes in the period and growth rate of ENSO (Fedorov and Philander 2000).

A very strong asymmetry between TIO+ and TIO− is also seen in the wind response in the western equatorial Pacific and off-equatorial regions. Wind changes in these regions have the potential to influence the mean state circulation in the Pacific and properties of water and heat exchanged between the extratropics and tropics (Zeller et al. 2021) along with the characteristics of ENSO (Fedorov and Philander

2000). Detailed understanding of the effects of such asymmetries on the oceanic circulation requires further investigation with an ocean general circulation model.

Using our idealized simulations, we have identified several asymmetries that could help to explain the recent decline of the TIO− TPO pan-tropical connection. First, our results show that for the TIO+ phase, which is the Indian Ocean warming phase that we are currently experiencing, the pan-tropical Indian-Pacific connection is significantly weaker than that seen in the TIO− phase. This asymmetry is apparent in Pacific basin average and northwestern Pacific region precipitation, zonal wind, and wind speed responses, particularly, in the northwestern (110°–175°E, 6°–22°N) and equatorial western Pacific (125°–169°E, 0°–5°N) regions (Figs. 7, 8d, and 9a,c). Although it is unclear precisely how much impact these apparent asymmetries would have on the TPO response in a coupled setting, the asymmetries identified here may be able to explain at least some portion of the recent observed decline in TIO influence on the TPO (Cai et al. 2019; Han and Wang 2021). However, as this is a single model study forced with fixed SSTs (i.e., in an uncoupled setting), our results may need confirmation with other models in both the AGCM forced and coupled setting.

Acknowledgments. All authors acknowledge the Australian Research Council (ARC) Centre of Excellence for Climate Extremes (Grant CE170100023) for supporting this research. Shayne McGregor acknowledges support from the ARC through Grants FT160100162 and DP200102329. Martin Singh acknowledges support from the ARC through Grants DE190100866 and DP200102954. This research was undertaken with the assistance of resources and services from the National Computational Infrastructure (NCI), which is supported by the Australian Government. We thank all three reviewers and the editor for their very thoughtful and constructive feedback on this manuscript. The authors have no conflicts to disclose.

Data availability statement. The data and scripts used in this work are available from the corresponding author upon reasonable request.

REFERENCES

Abellán, E., S. McGregor, M. H. England, and A. Santoso, 2018: Distinctive role of ocean advection anomalies in the development of the extreme 2015–16 El Niño. *Climate Dyn.*, **51**, 2191–2208, https://doi.org/10.1007/s00382-017-4007-0.

Ault, T. R., C. Deser, M. Newman, and J. Emile-Geay, 2013: Characterizing decadal to centennial variability in the equatorial Pacific during the last millennium. *Geophys. Res. Lett.*, **40**, 3450–3456, https://doi.org/10.1002/grl.50647.

Back, L. E., and C. S. Bretherton, 2009: A simple model of climatological rainfall and vertical motion patterns over the tropical oceans. *J. Climate*, **22**, 6477–6497, https://doi.org/10.1175/2009JCLI2393.1.

Bi, D., and Coauthors, 2013: The access coupled model: Description, control climate and evaluation. *Aust. Meteor. Oceanogr. J.*, **63**, 41–64, https://doi.org/10.22499/2.6301.004.

Bjerknes, J., 1969: Atmospheric teleconnections from the equatorial Pacific. *Mon. Wea. Rev.*, **97**, 163–172, https://doi.org/10.1175/1520-0493(1969)097<0163:ATFTEP>2.3.CO;2.

Cai, W., P. H. Whetton, and A. B. Pittock, 2001: Fluctuations of the relationship between ENSO and northeast Australian rainfall. *Climate Dyn.*, **17**, 421–432, https://doi.org/10.1007/PL00013738.

——, and Coauthors, 2019: Pantropical climate interactions. *Science*, **363**, eaav4236, https://doi.org/10.1126/science.aav4236.

Capotondi, A., and P. D. Sardeshmukh, 2015: Optimal precursors of different types of ENSO events. *Geophys. Res. Lett.*, **42**, 9952–9960, https://doi.org/10.1002/2015GL066171.

——, ——, and L. Ricciardulli, 2018: The nature of the stochastic wind forcing of ENSO. *J. Climate*, **31**, 8081–8099, https://doi.org/10.1175/JCLI-D-17-0842.1.

Dhame, S., A. S. Taschetto, A. Santoso, and K. J. Meissner, 2020: Indian Ocean warming modulates global atmospheric circulation trends. *Climate Dyn.*, **55**, 2053–2073, https://doi.org/10.1007/s00382-020-05369-1.

England, M. H., and Coauthors, 2014: Recent intensification of wind-driven circulation in the Pacific and the ongoing warming hiatus. *Nat. Climate Change*, **4**, 222–227, https://doi.org/10.1038/nclimate2106.

Fedorov, A. V., and S. G. Philander, 2000: Is El Niño changing? *Science*, **288**, 1997–2002, https://doi.org/10.1126/science.288.5473.1997.

Funk, C., M. D. Dettinger, J. C. Michaelsen, J. P. Verdin, M. E. Brown, M. Barlow, and A. Hoell, 2008: Warming of the Indian Ocean threatens eastern and southern African food security but could be mitigated by agricultural development. *Proc. Natl. Acad. Sci. USA*, **105**, 11 081–11 086, https://doi.org/10.1073/pnas.0708196105.

Gill, A. E., 1980: Some simple solutions for heat-induced tropical circulation. *Quart. J. Roy. Meteor. Soc.*, **106**, 447–462, https://doi.org/10.1002/qj.49710644905.

Ham, Y.-G., J.-S. Kug, J.-Y. Park, and F.-F. Jin, 2013: Sea surface temperature in the north tropical Atlantic as a trigger for El Niño/Southern Oscillation events. *Nat. Geosci.*, **6**, 112–116, https://doi.org/10.1038/ngeo1686.

Han, X., and C. Wang, 2021: Weakened feedback of the Indian Ocean on El Niño since the early 1990s. *Climate Dyn.*, **57**, 879–894, https://doi.org/10.1007/s00382-021-05745-5.

Inoue, K., Á. F. Adames, and K. Yasunaga, 2020: Vertical velocity profiles in convectively coupled equatorial waves and MJO: New diagnoses of vertical velocity profiles in the wavenumber–frequency domain. *J. Atmos. Sci.*, **77**, 2139–2162, https://doi.org/10.1175/JAS-D-19-0209.1.

Izumo, T., J. Vialard, H. Dayan, M. Lengaigne, and I. Suresh, 2016: A simple estimation of equatorial Pacific response from windstress to untangle Indian Ocean dipole and basin influences on El Niño. *Climate Dyn.*, **46**, 2247–2268, https://doi.org/10.1007/s00382-015-2700-4.

Karamperidou, C., and Coauthors, 2020: ENSO in a changing climate: Challenges, paleo-perspectives, and outlook. *El Niño Southern Oscillation in a Changing Climate*, *Geophys. Monogr.*, Vol. 253, Amer. Geophys. Union, 471–484, https://doi.org/10.1002/9781119548164.ch21.

Kido, S., I. Richter, T. Tozuka, and P. Chang, 2023: Understanding the interplay between ENSO and related tropical SST variability using linear inverse models. *Climate Dyn.*, **61**, 1029–1048, https://doi.org/10.1007/s00382-022-06484-x.

Kosaka, Y., and S.-P. Xie, 2013: Recent global-warming hiatus tied to equatorial Pacific surface cooling. *Nature*, **501**, 403–407, https://doi.org/10.1038/nature12534.

Kug, J.-S., and I.-S. Kang, 2006: Interactive feedback between ENSO and the Indian Ocean. *J. Climate*, **19**, 1784–1801, https://doi.org/10.1175/JCLI3660.1.

——, T. Li, S.-I. An, I.-S. Kang, J.-J. Luo, S. Masson, and T. Yamagata, 2006: Role of the ENSO–Indian Ocean coupling on ENSO variability in a coupled GCM. *Geophys. Res. Lett.*, **33**, L09710, https://doi.org/10.1029/2005GL024916.

Lee, S.-K., D. Kim, G. R. Foltz, and H. Lopez, 2020: Pantropical response to global warming and the emergence of a La Niña-like mean state trend. *Geophys. Res. Lett.*, **47**, e2019GL086497, https://doi.org/10.1029/2019GL086497.

Li, G., and B. Ren, 2012: Evidence for strengthening of the tropical Pacific Ocean surface wind speed during 1979–2001. *Theor. Appl. Climatol.*, **107**, 59–72, https://doi.org/10.1007/s00704-011-0463-3.

Li, X., S.-P. Xie, S. T. Gille, and C. Yoo, 2016: Atlantic-induced pan-tropical climate change over the past three decades. *Nat. Climate Change*, **6**, 275–279, https://doi.org/10.1038/nclimate2840.

Liguori, G., S. McGregor, J. M. Arblaster, M. S. Singh, and G. A. Meehl, 2020: A joint role for forced and internally-driven variability in the decadal modulation of global warming. *Nat. Commun.*, **11**, 3827, https://doi.org/10.1038/s41467-020-17683-7.

Luo, J.-J., R. Zhang, S. K. Behera, Y. Masumoto, F.-F. Jin, R. Lukas, and T. Yamagata, 2010: Interaction between El Niño and extreme Indian Ocean dipole. *J. Climate*, **23**, 726–742, https://doi.org/10.1175/2009JCLI3104.1.

——, W. Sasaki, and Y. Masumoto, 2012: Indian Ocean warming modulates Pacific climate change. *Proc. Natl. Acad. Sci. USA*, **109**, 18 701–18 706, https://doi.org/10.1073/pnas.1210239109.

Maher, N., A. S. Gupta, and M. H. England, 2014: Drivers of decadal hiatus periods in the 20th and 21st centuries. *Geophys. Res. Lett.*, **41**, 5978–5986, https://doi.org/10.1002/2014GL060527.

——, D. Matei, S. Milinski, and J. Marotzke, 2018: ENSO change in climate projections: Forced response or internal variability? *Geophys. Res. Lett.*, **45**, 11 390–11 398, https://doi.org/10.1029/2018GL079764.

McGregor, S., N. J. Holbrook, and S. B. Power, 2007: Interdecadal sea surface temperature variability in the equatorial Pacific Ocean. Part I: The role of off-equatorial wind stresses and oceanic Rossby waves. *J. Climate*, **20**, 2643–2658, https://doi.org/10.1175/JCLI4145.1.

——, A. Timmermann, N. Schneider, M. F. Stuecker, and M. H. England, 2012: The effect of the South Pacific convergence zone on the termination of El Niño events and the meridional asymmetry of ENSO. *J. Climate*, **25**, 5566–5586, https://doi.org/10.1175/JCLI-D-11-00332.1.

——, N. Ramesh, P. Spence, M. H. England, M. J. McPhaden, and A. Santoso, 2013: Meridional movement of wind anomalies during ENSO events and their role in event termination. *Geophys. Res. Lett.*, **40**, 749–754, https://doi.org/10.1002/grl.50136.

——, A. Timmermann, M. F. Stuecker, M. H. England, M. Merrifield, F.-F. Jin, and Y. Chikamoto, 2014: Recent Walker circulation strengthening and Pacific cooling amplified by Atlantic warming. *Nat. Climate Change*, **4**, 888–892, https://doi.org/10.1038/nclimate2330.

McPhaden, M. J., S. E. Zebiak, and M. H. Glantz, 2006: ENSO as an integrating concept in Earth science. *Science*, **314**, 1740–1745, https://doi.org/10.1126/science.1132588.

——, T. Lee, S. Fournier, and M. A. Balmaseda, 2020a: ENSO observations. *El Niño Southern Oscillation in a Changing Climate*, *Geophys. Monogr.*, Vol. 253, Amer. Geophys. Union, 39–63, https://doi.org/10.1002/9781119548164.ch3.

——, A. Santoso, and W. Cai, Eds., 2020b: *El Niño Southern Oscillation in a Changing Climate*, *Geophys. Monogr.*, Vol. 253, Amer. Geophys. Union, 506 pp., https://doi.org10.1002/9781119548164.

Meehl, G., and Coauthors, 2019: Mutually interactive decadal-timescale processes connecting the tropical Atlantic and Pacific. *2019 Fall Meeting*, San Francisco, CA, Amer. Geophys. Union, Abstract OS23A-01, https://ui.adsabs.harvard.edu/abs/2019AGUFMOS23A..01M/abstract.

Merrifield, M. A., 2011: A shift in western tropical Pacific sea level trends during the 1990s. *J. Climate*, **24**, 4126–4138, https://doi.org/10.1175/2011JCLI3932.1.

Mishra, V., B. V. Smoliak, D. P. Lettenmaier, and J. M. Wallace, 2012: A prominent pattern of year-to-year variability in Indian summer monsoon rainfall. *Proc. Natl. Acad. Sci. USA*, **109**, 7213–7217, https://doi.org/10.1073/pnas.1119150109.

Naha, R., 2022: Interbasin influences on the Pacific basin mean state. Ph.D. thesis, Monash University, 137 pp., https://bridges.monash.edu/articles/thesis/Interbasin_Influences_on_the_Pacific_Basin_Mean_State/22339624.

Neelin, J. D., D. S. Battisti, A. C. Hirst, F.-F. Jin, Y. Wakata, T. Yamagata, and S. E. Zebiak, 1998: ENSO theory. *J. Geophys. Res.*, **103**, 14 261–14 290, https://doi.org/10.1029/97JC03424.

Neske, S., and S. McGregor, 2018: Understanding the warm water volume precursor of ENSO events and its interdecadal variation. *Geophys. Res. Lett.*, **45**, 1577–1585, https://doi.org/10.1002/2017GL076439.

Ohba, M., and H. Ueda, 2007: An impact of SST anomalies in the Indian Ocean in acceleration of the El Niño to La Niña transition. *J. Meteor. Soc. Japan*, **85**, 335–348, https://doi.org/10.2151/jmsj.85.335.

Okumura, Y. M., M. Ohba, C. Deser, and H. Ueda, 2011: A proposed mechanism for the asymmetric duration of El Niño and La Niña. *J. Climate*, **24**, 3822–3829, https://doi.org/10.1175/2011JCLI3999.1.

Palmer, T., 2019: Stochastic weather and climate models. *Nat. Rev. Phys.*, **1**, 463–471, https://doi.org/10.1038/s42254-019-0062-2.

Power, S., and R. Colman, 2006: Multi-year predictability in a coupled general circulation model. *Climate Dyn.*, **26**, 247–272, https://doi.org/10.1007/s00382-005-0055-y.

——, and Coauthors, 2021: Decadal climate variability in the tropical Pacific: Characteristics, causes, predictability, and prospects. *Science*, **374**, eaay9165, https://doi.org/10.1126/science.aay9165.

Ren, H.-L., J. Zuo, F.-F. Jin, and M. F. Stuecker, 2016: ENSO and annual cycle interaction: The combination mode representation in CMIP5 models. *Climate Dyn.*, **46**, 3753–3765, https://doi.org/10.1007/s00382-015-2802-z.

Ruprich-Robert, Y., R. Msadek, F. Castruccio, S. Yeager, T. Delworth, and G. Danabasoglu, 2017: Assessing the climate impacts of the observed Atlantic multidecadal variability using the GFDL CM2.1 and NCAR CESM1 global coupled models. *J. Climate*, **30**, 2785–2810, https://doi.org/10.1175/JCLI-D-16-0127.1.

Schumacher, C., and R. A. Houze Jr., 2003a: Stratiform rain in the tropics as seen by the TRMM Precipitation Radar. *J. Climate*, **16**, 1739–1756, https://doi.org/10.1175/1520-0442(2003)016<1739:SRITTA>2.0.CO;2.

——, and ——, 2003b: The TRMM Precipitation Radar's view of shallow, isolated rain. *J. Appl. Meteor.*, **42**, 1519–1524, https://doi.org/10.1175/1520-0450(2003)042<1519:TTPRVO>2.0.CO;2.

Singh, M. S., and P. A. O'Gorman, 2013: Influence of entrainment on the thermal stratification in simulations of radiative-convective equilibrium. *Geophys. Res. Lett.*, **40**, 4398–4403, https://doi.org/10.1002/grl.50796.

Stuecker, M. F., A. Timmermann, F.-F. Jin, S. McGregor, and H.-L. Ren, 2013: A combination mode of the annual cycle and the El Niño/Southern Oscillation. *Nat. Geosci.*, **6**, 540–544, https://doi.org/10.1038/ngeo1826.

——, F.-F. Jin, A. Timmermann, and S. McGregor, 2015: Combination mode dynamics of the anomalous northwest Pacific anticyclone. *J. Climate*, **28**, 1093–1111, https://doi.org/10.1175/JCLI-D-14-00225.1.

——, A. Timmermann, F.-F. Jin, Y. Chikamoto, W. Zhang, A. T. Wittenberg, E. Widiasih, and S. Zhao, 2017: Revisiting ENSO/Indian Ocean dipole phase relationships. *Geophys. Res. Lett.*, **44**, 2481–2492, https://doi.org/10.1002/2016GL072308.

Tao, L., L. Wu, Y. Wang, and J. Yang, 2012: Influence of tropical Indian Ocean warming and ENSO on tropical cyclone activity over the western North Pacific. *J. Meteor. Soc. Japan*, **90**, 127–144, https://doi.org/10.2151/jmsj.2012-107.

Taylor, K. E., D. Williamson, and F. Zwiers, 2000: The sea surface temperature and sea-ice concentration boundary conditions for AMIP II simulations. Program for Climate Model Diagnosis and Intercomparison Rep. 60, 28 pp., https://pcmdi.llnl.gov/report/ab60.html.

Timmermann, A., J. Oberhuber, A. Bacher, M. Esch, M. Latif, and E. Roeckner, 1999: Increased El Niño frequency in a climate model forced by future greenhouse warming. *Nature*, **398**, 694–697, https://doi.org/10.1038/19505.

——, and Coauthors, 2018: El Niño–Southern Oscillation complexity. *Nature*, **559**, 535–545, https://doi.org/10.1038/s41586-018-0252-6.

Trenberth, K. E., and T. J. Hoar, 1997: El Niño and climate change. *Geophys. Res. Lett.*, **24**, 3057–3060, https://doi.org/10.1029/97GL03092.

Ueda, H., Y. Kamae, M. Hayasaki, A. Kitoh, S. Watanabe, Y. Miki, and A. Kumai, 2015: Combined effects of recent Pacific cooling and Indian Ocean warming on the Asian monsoon. *Nat. Commun.*, **6**, 8854, https://doi.org/10.1038/ncomms9854.

Vimont, D. J., 2005: The contribution of the interannual ENSO cycle to the spatial pattern of decadal ENSO-like variability. *J. Climate*, **18**, 2080–2092, https://doi.org/10.1175/JCLI3365.1.

Wang, B., R. Wu, and R. Lukas, 1999: Roles of the western North Pacific wind variation in thermocline adjustment and ENSO phase transition. *J. Meteor. Soc. Japan*, **77** (1), 1–16, https://doi.org/10.2151/jmsj1965.77.1_1.

——, X. Luo, Y.-M. Yang, W. Sun, M. A. Cane, W. Cai, S.-W. Yeh, and J. Liu, 2019: Historical change of El Niño properties sheds light on future changes of extreme El Niño. *Proc. Natl. Acad. Sci. USA*, **116**, 22 512–22 517, https://doi.org/10.1073/pnas.1911130116.

Wang, C., 2019: Three-ocean interactions and climate variability: A review and perspective. *Climate Dyn.*, **53**, 5119–5136, https://doi.org/10.1007/s00382-019-04930-x.

Wang, L., J.-Y. Yu, and H. Paek, 2017: Enhanced biennial variability in the Pacific due to Atlantic capacitor effect. *Nat. Commun.*, **8**, 14887, https://doi.org/10.1038/ncomms14887.

Weisberg, R. H., and C. Wang, 1997: A western Pacific oscillator paradigm for the El Niño-Southern Oscillation. *Geophys. Res. Lett.*, **24**, 779–782, https://doi.org/10.1029/97GL00689.

Williams, A. I. L., N. Jeevanjee, and J. Bloch-Johnson, 2023: Circus tents, convective thresholds, and the non-linear climate response to tropical SSTs. *Geophys. Res. Lett.*, **50**, e2022GL101499, https://doi.org/10.1029/2022GL101499.

Xie, S.-P., K. Hu, J. Hafner, H. Tokinaga, Y. Du, G. Huang, and T. Sampe, 2009: Indian Ocean capacitor effect on Indo–western Pacific climate during the summer following El Niño. *J. Climate*, **22**, 730–747, https://doi.org/10.1175/2008JCLI2544.1.

Yano, J.-I., and R. Plant, 2012: Interactions between shallow and deep convection under a finite departure from convective quasi equilibrium. *J. Atmos. Sci.*, **69**, 3463–3470, https://doi.org/10.1175/JAS-D-12-0108.1.

Yeh, S.-W., J.-S. Kug, B. Dewitte, M.-H. Kwon, B. P. Kirtman, and F.-F. Jin, 2009: El Niño in a changing climate. *Nature*, **461**, 511–514, https://doi.org/10.1038/nature08316.

Yun, K.-S., and A. Timmermann, 2018: Decadal monsoon–ENSO relationships reexamined. *Geophys. Res. Lett.*, **45**, 2014–2021, https://doi.org/10.1002/2017GL076912.

Zelle, H., G. Appeldoorn, G. Burgers, and G. J. van Oldenborgh, 2004: The relationship between sea surface temperature and thermocline depth in the eastern equatorial Pacific. *J. Phys. Oceanogr.*, **34**, 643–655, https://doi.org/10.1175/2523.1.

Zeller, M., S. McGregor, E. van Sebille, A. Capotondi, and P. Spence, 2021: Subtropical-tropical pathways of spiciness anomalies and their impact on equatorial Pacific temperature. *Climate Dyn.*, **56**, 1131–1144, https://doi.org/10.1007/s00382-020-05524-8.

Zhang, Y., J. M. Wallace, and D. S. Battisti, 1997: ENSO-like interdecadal variability: 1900–93. *J. Climate*, **10**, 1004–1020, https://doi.org/10.1175/1520-0442(1997)010<1004:ELIV>2.0.CO;2.

Zheng, X.-T., S.-P. Xie, and Q. Liu, 2011: Response of the Indian Ocean basin mode and its capacitor effect to global warming. *J. Climate*, **24**, 6146–6164, https://doi.org/10.1175/2011JCLI4169.1.

Zhuang, Y., R. Fu, J. A. Marengo, and H. Wang, 2017: Seasonal variation of shallow-to-deep convection transition and its link to the environmental conditions over the central Amazon. *J. Geophys. Res. Atmos.*, **122**, 2649–2666, https://doi.org/10.1002/2016JD025993.